Journal of Molecular Spectroscopy **206,** 62–72 (2001)
doi:10.1006/jmsp.2000.8289, available online at http://www.idealibrary.com on IDEAL®

Fourier Transform Spectroscopy of the BaI Molecule: Simultaneous Analysis of Seven Electronic States Including the $D\,^2\Sigma^+$ and the $G\,^2\Sigma^+$ States

R. F. Gutterres,*,† C. E. Fellows,† J. Vergès,* and C. Amiot*,[1]

*Laboratoire Aimé Cotton,[2] Bât 505, Campus d'Orsay, 91405, Orsay Cedex, France; and †Laboratório de Espectroscopia e Laser, Universidade Federal Fluminense, Campus da Boa Viagem, Niterói, RJ, 24210-340, Brazil

Received September 15, 2000; in revised form November 30, 2000

In this work, the BaI $D^2\Sigma^+$ and $G^2\Sigma^+$ electronic states were investigated using laser-induced fluorescence (LIF) and Fourier transform spectroscopy (FTS). The LIF visible spectra were obtained by using the second harmonic of the Ti:sapphire single-mode laser and the Ar^+ and Kr^+ multimode lasers as excitation sources. Previously recorded data, taken from C. A. Leach, A. A. Tsekouras, and R. N. Zare (1992, *J. Mol. Spectrosc*. **153**, 59–72) and from R. F. Gutterres, J. Vergès, and C. Amiot (1999, *J. Mol. Spectrosc*. **196**, 29–44; 2000, *J. Mol. Spectrosc*. **200**, 253–260; and 2000, *J. Mol. Spectrosc*. **201**, 326–327) were combined with the present data. Accurate and improved molecular constants for the $X^2\Sigma^+$, $B^2\Sigma^+$, $A'^2\Delta$, $A^2\Pi$, $C^2\Pi$, and $D^2\Sigma^+$ states and 16 term values of the $G^2\Sigma^+$ state were derived from a simultaneous treatment of the whole data set (12 684 transitions) with a standard deviation of 3.26×10^{-3} cm^{-1}.

Key Words: Fourier transform spectroscopy; laser-induced fluorescence; analysis of seven electronic states of BaI molecule; molecular constants.

I. INTRODUCTION

The alkaline-earth monohalides are a widely researched theme among theoretical and experimental spectroscopists. The electronic structure of the ground electronic state and the structures of the first excited electronic states can be described by an unpaired electron and a molecular ion core consisting of two closed shell ions M^{2+} and X^-. Thus it can be expected, from a theoretical point of view, that the electronic structure of these radicals should have a behavior similar to that of the electronic structure of the alkali atoms. Different ionic bonding models have been developed to represent the structure of these first excited states, e.g., the *electrostatic polarization model* (*1, 2*), the *ligand-field approach* (*3*), and the *quantum defect theory* (*4*). From these models, predictions for the transition energies and for the permanent and transition dipole moments have been done for several alkaline-earth monohalide molecules, including the BaI molecule (*5–7*).

The BaI molecule was first identified in 1928 by Walters and Barratt (*8*), who have observed the absorption spectrum of the $C^2\Pi$–$X^2\Sigma^+$ band system. Later, the bandheads of both spin–orbit components of the $C^2\Pi$–$X^2\Sigma^+$ band system were studied by Mesnage (*9*). Patel and Shah (*10*) have observed the same band system and recognized that the absorption spectrum in the region of 380 nm, observed by Walters and Barratt (*8*), was caused by two other electronic band systems: $E^2\Sigma^+$–$X^2\Sigma^+$ at about 374 nm and $D^2\Sigma^+$–$X^2\Sigma^+$ at about 388 nm. Rao *et al*. (*11*) have obtained an improved set of vibrational constants for the $X^2\Sigma^+$ and the $C^2\Pi$ states. Bradford *et al*. (*12*) have observed the chemiluminescence reaction $Ba + I_2$ and have determined that the infrared emission was issued from two unobserved electronic transitions: $A^2\Pi$–$X^2\Sigma^+$ and $B^2\Pi$–$X^2\Sigma^+$. In all the above-mentioned works the experiments were unable to resolve the individual rotational transitions, which are very closely spaced, due mainly to the fact that the large mass of barium and iodine atoms results in very small rotational constants.

It was only after the early 1980s that a systematic and accurate study of the $C^2\Pi$–$X^2\Sigma^+$ band system with rotational resolution was carried out. The $C^2\Pi$–$X^2\Sigma^+$ (0–0) band was studied by using population-labeling optical–optical double resonance (PLOODR) first by Johnson *et al*. (*13*) and after that by Johnson and Zare (*14*). The same band has also been studied by using selectively detected laser-induced fluorescence (SDLIF) by Johnson *et al*. (*15*). In these works (*13–15*), a collimated beam of the BaI molecule obtained from an oven source was used and the reported rotational constants were found to be essentially equal to each other. A remarkable study of the $C^2\Pi$–$X^2\Sigma^+$ (0–0) band, in which high rotational levels (J'' up to nearly 500) were observed, has been performed by Zhao *et al*. (*16*). In their work a crossed-beam apparatus, SDLIF and laser-induced fluorescence (LIF), were used. From the obtained data set, and combining with previous results (*13–15*), it was possible for the authors to determine an improved and a more general set of molecular constants. Using PLOODR, Leach *et al*. (*17*) have

[1] To whom correspondence should be addressed. Fax: (33) 1 69 35 21 00. E-mail: Claude.Amiot@lac.u-psud.fr.

[2] Laboratoire Aimé Cotton is in association with Université Paris Sud, Orsay.

0022-2852/01 $35.00

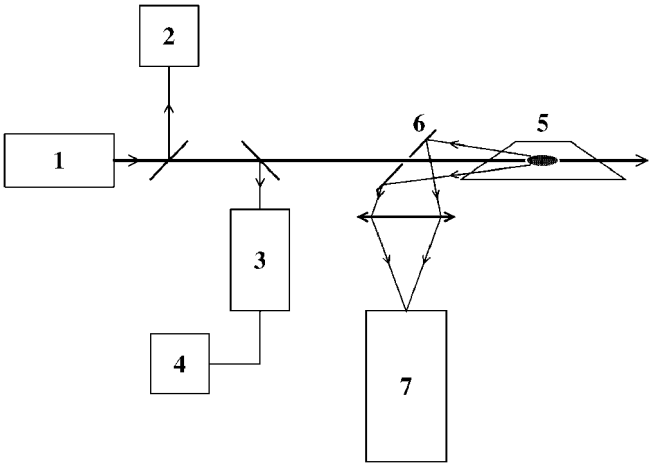

FIG. 1. Schematic diagram of the experimental setup. (1) Laser source (2× Ti:sapphire, Ar^+ or Kr^+ laser). (2) Lambdameter. (3) Fabry–Perot spectrum analyzer. (4) Oscilloscope recording the transmission fringes of the spectrum analyzer. (5) Heat pipe oven. (6) Pierced mirror collecting the uorescence light backward with respect to the laser beam. (7) Two-meter optical path length Fourier transform spectrometer. Devices 2, 3, and 4 were not used in the experiments with Ar^+ and Kr^+ lasers.

observed and assigned the $C^2\Pi$–$X^2\Sigma^+$ (8–8) band. Finally, Leach *et al.* (*18*) have performed a general rovibrational analysis of the BaI $C^2\Pi$–$X^2\Sigma^+$ band system with $v \leq 12$. The observed bands ($\Delta v = 0$), with $v = 0$, 1, 4, 8, and 12, were recorded by SDLIF and, in addition, the bands ($\Delta v = 0$), with $v = 0$, 1, 2, and 3, were measured by LIF, in which the undispersed fluorescence was detected. The obtained data were combined with previous results (*14, 15, 17*) as well as with the microwave measurements of low J'' values for $v = 0$–5 of the $X^2\Sigma^+$ state obtained by Töring and Döbl (*19*). A set of 31 molecular constants was calculated from a weighted nonlinear fit; it reproduced the 5032 observed transition wavenumbers with a standard deviation of 2.37×10^{-3} cm^{-1}. The values obtained for these constants (*18*) improved the values obtained by Rao *et al.* (*11*).

The spectroscopic knowledge of the BaI molecule has been largely improved in the Past 2 years. By using Fourier transform spectroscopy (FTS) combined with thermal emission and LIF, generated from a Ti:sapphire single-mode laser, Gutterres *et al.* (*20*) have assigned more than 2400 observed wavenumbers of the $B^2\Sigma^+$–$X^2\Sigma^+$ band system. From a global analysis, including the data from (*18*), a set of 51 molecular constants was calculated, which reproduced the $B^2\Sigma^+$–$X^2\Sigma^+$ and $C^2\Pi$–$X^2\Sigma^+$ band system spectral data, with a standard deviation of less than 2.3×10^{-3} cm^{-1}. The several observed transitions with $\Delta v \neq 0$ have allowed the authors to solve the pure vibrational terms of the Hamiltonian used by Leach *et al.* (*18*). After that, the $A^2\Pi$ electronic state was investigated by using LIF and FTS (*21*). Near-infrared and visible spectra were obtained from the Ti:sapphire and dye single-mode laser excitations, from a Kr^+ multimode ion laser excitation, and also from thermal emission. Rotationally resolved data, originating from 19 vibrational levels of the $A^2\Pi$ state, were added to previous results (*18, 20*) and used in the final analysis. Accurate molecular constants for all involved states could be derived from a simultaneous treatment of the whole data set. Finally, using LIF combined with FTS, Gutterres *et al.* (*22*) have carried out the first spectroscopic study with high resolution of the $\Omega = 3/2$ component of the BaI $A'^2\Delta$ electronic state. Several rotationally resolved transitions involving 16 vibrational levels of the $A'^2\Delta_{3/2}$ component could be assigned. A simultaneous analysis including previously reported data (*18, 20, 21*) was done and a set of 9 molecular constants for the $A'^2\Delta_{3/2}$ component was determined.

In this work a spectroscopic study of the BaI molecule, including the $D^2\Sigma^+$ and the $G^2\Sigma^+$ states, is presented. The $D^2\Sigma^+$–$A^2\Pi$, $D^2\Sigma^+$–$B^2\Sigma^+$, $G^2\Sigma^+$–$A^2\Pi$, and $G^2\Sigma^+$–$B^2\Sigma^+$ band systems were investigated by using LIF and FTS. The visible LIF spectra were obtained by using as laser sources the second harmonic of a single-mode Ti:sapphire laser and the Ar^+ and Kr^+ multimode lasers. Previously recorded data of the $A^2\Pi$–$X^2\Sigma^+$, $B^2\Sigma^+$–$X^2\Sigma^+$, $C^2\Pi$–$A^2\Pi$, $C^2\Pi$–$A'^2\Delta$, $C^2\Pi$–$B^2\Sigma^+$, and $C^2\Pi$–$X^2\Sigma^+$, band systems, taken from (*18, 20–22*), were added to the present work data field. Rotationally resolved data,

TABLE 1
Vacuum Wavenumber σ and Emitted Power P of the Laser Radiation Sources Used

Laser	σ (cm^{-1})	P (W)	σ (cm^{-1})	P(W)
2×Ti:Sa	26437.72	0.3	26439.55	0.3
	26453.53	0.3	26480.95	0.3
	26482.47	0.3	-	-
Kr^+	29621.47	0.2	-	-
Ar^+	29966.26	0.4	29889.31	0.4
	29766.76	0.4	-	-

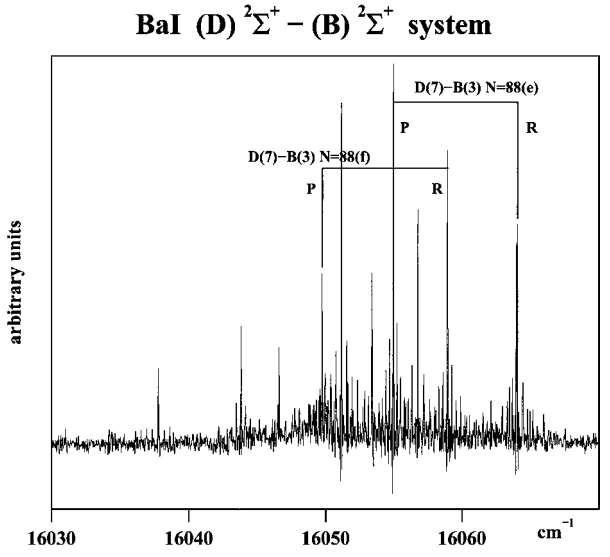

FIG. 2. Part of the *D–B* LIF spectrum induced by the 26 437.72 cm^{-1} laser line (second harmonic of the Ti:sapphire).

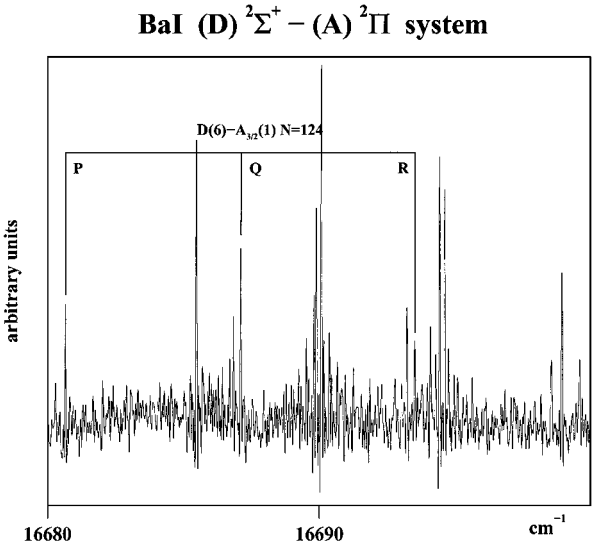

FIG. 3. Part of the *D–A* LIF spectrum induced by the 26 437.72 cm^{-1} laser line (second harmonic of the Ti:sapphire).

originating from 12 vibrational levels ($5 \leq v \leq 16$) of the $D^2\Sigma^+$ state, 2 undetermined vibrational levels of the $G^2\Sigma^+$ state, 32 vibrational levels ($0 \leq v \leq 31$) of the ground state, 19 vibrational levels ($0 \leq v \leq 5$ and $7 \leq v \leq 19$) of the $A^2\Pi$ state, 16 vibrational levels ($0 \leq v \leq 3$ and $7 \leq v \leq 18$) of the $A'^2\Delta_{3/2}$ component, 24 vibrational levels ($0 \leq v \leq 19, 21 \leq v \leq 19$ and $v = 26$) of the $B^2\Sigma^+$ state, and 12 vibrational levels ($0 \leq v \leq 4, 8 \leq v \leq 14$) of the $C^2\Pi$ state, were used in the final analysis. Accurate molecular constants for the $X^2\Sigma^+$, $A'^2\Delta_{3/2}$, $A^2\Pi$, $B^2\Sigma^+$, $C^2\Pi$, and $D^2\Sigma^+$ states, as well as 16 term values of the $G^2\Sigma^+$ state, were derived from a simultaneous treatment of the whole data set.

II. THE EXPERIMENT

The BaI molecules were produced in a heat pipe oven. This molecular source was proposed by Vidal and Cooper (*23*) and it has been largely used in experimental studies of alkaline-earth monohalides like BaCl (*24–27*), BaBr (*28*), BaF (*29*, *30*), CaF (*31*), and BaI (*20–22*). In the recording of the spectra, a mixture of a few grams of Ba metal and BaI_2 powder was heated to 850°C in the presence of 12 mbar of argon buffer gas. The obtained emission was focused onto the entrance iris of a 2-m optical path length Fourier transform spectrometer. A schematic diagram of the experimental setup is shown in Fig. 1.

The excitation of the BaI molecules was done using five laser lines provided by a frequency doubler (Laser Analytical Systems—Wavetrain High efficiency PM) of a Ti:sapphire single-mode laser (Coherent 899-21), associated with an Ar^+ laser (Coherent Innova K 3000). Also four laser lines provided by an Ar^+ and a Kr^+ (Coherent Innova K 3000 and Spectra-Physics 171-19) multimode ion laser were used in the excitation of the molecules. The stability of all used laser lines, in both intensity and frequency, was sufficiently high during the recording time of the spectra (about 2 h). Table 1 shows the spectral characteristics, vacuum wavenumbers, and emitted power of all laser lines used.

The fluorescence spectra, induced by the Ti:sapphire laser frequency-doubled lines, were recorded in the region between 15 000 and 18 300 cm^{-1}. For the lines provided by the Ar^+ and Kr^+ lasers the resulting fluorescence spectra were recorded

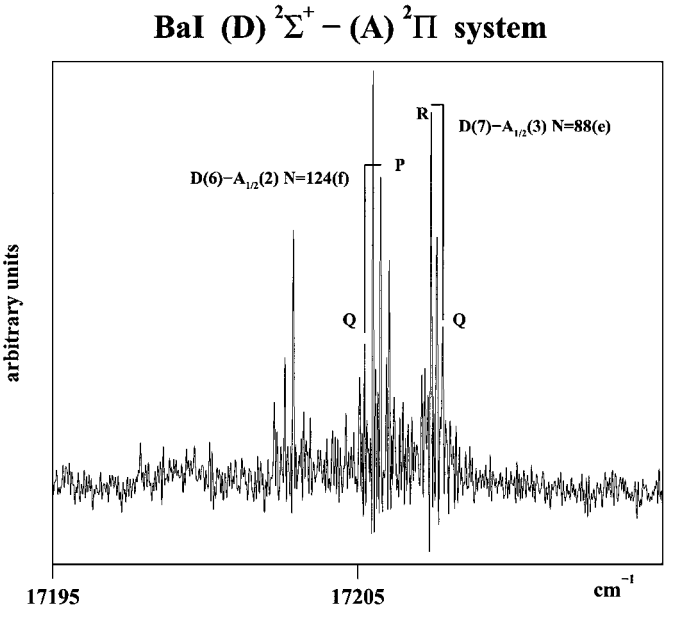

FIG. 4. Part of the *D–A* LIF spectrum induced by the 26 437.72 cm^{-1} laser line (second harmonic of the Ti:sapphire).

TABLE 2

Vacuum Wavenumbers of the Doubled Ti:Sapphire Single-Mode Laser σ, Quantum Numbers v', J' and Energy E' for the $D^2\Sigma^+$ Excited Levels, and Quantum Numbers v'', J'' and Energy E'' of the Lower Levels in the Ground $X^2\Sigma^+$ State (Range of Observed v Values in the $A^2\Pi$ and $B^2\Sigma^+$ States)

$\sigma(cm^{-1})$	v'	J'	$E'(cm^{-1})$	v''	J''	$E''(cm^{-1})$	Δv^a	Δv^b
26437.72	5	149.5	27276.35	1	150.5	838.69	1-12	1-8
	5	150.5	27276.69	1	151.5	839.07	1-12	1-5
	6	123.5	27235.03	2	124.5	797.31	1-10	1-9
	6	124.5	27235.31	2	125.5	797.59	1-10	2-9
	7	87.5	27179.50	3	88.5	741.78	5-12	1-10
	7	88.5	27179.79	3	89.5	741.97	5-12	1-10
26439.55	8	23.5	27136.00	4	24.5	696.45	1-8	2-6
	8	24.5	27137.37	4	25.5	697.82	1-8	2-6
	8	25.5	27138.79	4	26.5	699.24	1-8	2-6
	8	26.5	27140.27	4	27.5	700.72	1-8	2-6
	8	27.5	27141.81	4	28.5	702.26	1-8	2-6
	8	28.5	27143.40	4	29.5	703.85	1-8	2-6
26453.53	11	32.5	27609.08	7	33.5	1155.55	3-10	4-8
	11	33.5	27610.87	7	34.5	1157.34	3-10	4-8
	11	34.5	27612.72	7	35.5	1159.19	3-10	4-8
	11	35.5	27614.62	7	36.5	1161.09	3-10	4-8
	11	36.5	27616.58	7	37.5	1163.05	3-10	4-8
26480.95	8	182.5	27886.62	4	181.5	558.11	2-9	2-6
	9	229.5	28716.78	5	230.5	2235.83	4	3-8

[a] $A^2\Pi$ state.
[b] $B^2\Sigma^+$ state.

between 17 900 and 20 000 cm^{-1}. The unapodized resolution limit ranges from 0.005 to 0.02 cm^{-1}. The wavenumbers were calibrated relative to a fixed frequency reference line (*Xe* atomic transition near 3.5 μm) used to monitor the path difference of the interferometer. The absolute measurement uncertainty varied from 1×10^{-3} cm^{-1} for the strongest lines to 5×10^{-3} cm^{-1} for the weakest ones.

III. RESULTS

The previous knowledge (*20, 21*) of the $B^2\Sigma^+$ and $A^2\Pi$ states facilitated the assignment of the observed transitions. The excited D and G states possess a $^2\Sigma^+$ electronic structure, but the spectral feature of the $D^2\Sigma^+$–$B^2\Sigma^+$ and $G^2\Sigma^+$–$B^2\Sigma^+$ band systems, as well as of the $D^2\Sigma^+$–$A^2\Pi$ and $G^2\Sigma^+$–$A^2\Pi$ band systems, presents some important differences.

A. *The $D^2\Sigma^+$–$A^2\Pi_{1/2}$ and $D^2\Sigma^+$–$B^2\Sigma^+$ Band Systems*

Several doublets of P and R lines can be observed in Fig. 2, which shows a part of the recorded spectra of the $D^2\Sigma^+$–$B^2\Sigma^+$ band system. Each line is surrounded by collisional rotational relaxation lines with their intensities decreasing regularly and rapidly. The relative intensity of the P lines is stronger than the relative intensity of the R lines, when the transition comes from a level of the $D^2\Sigma^+$ that has e parity. The reverse is true when the transition comes from an f-type level.

The triplet structure of the $D^2\Sigma^+$–$A^2\Pi_{3/2}$ subband system can be seen in Fig. 3, which shows a part of the recorded spectra. The Q lines present a relative intensity stronger than the relative intensity of the P and R lines. Rotational relaxation lines are observed with a regular decrease in intensity. Figure 4 shows a part of the obtained spectra in which some transitions of the $D^2\Sigma^+$–$A^2\Pi_{1/2}$ band system are reproduced. The main fluorescence

TABLE 2—*Continued*

$\sigma(cm^{-1})$	v'	J'	$E'(cm^{-1})$	v''	J''	$E''(cm^{-1})$	Δv^a	Δv^b
26480.95	11	207.5	28754.95	7	208.5	2274.00	4-6	4-10
	13	121.5	28287.68	9	120.5	1806.73	6-11	5-7
	13	122.5	28287.95	9	121.5	1807.00	6	5-12
	14	108.5	28355.67	10	107.5	1874.72	7-10	7-14
	14	109.5	28355.91	10	108.5	1874.96	7-10	7-8
	14	174.5	28850.67	10	175.5	2369.22	-	7-10
	15	96.5	28432.50	11	95.5	1951.55	8-9	7-13
	16	151.5	28943.43	12	152.5	2462.48	5-11	9-14
26482.47	7	254.5	28745.27	3	255.5	2263.80	8	2-5
	7	255.5	28745.89	3	256.5	2263.42	-	2-5
	8	186.5	28079.41	4	185.5	1596.94	3	2-6
	8	187.5	28079.84	4	186.5	1597.37	2-9	2-6
	10	164.5	28162.97	6	163.5	1680.50	5	4-7
	11	151.5	28210.36	7	150.5	1727.88	4-10	4-10
	11	152.5	28210.70	7	149.5	1728.23	4-8	4-8
	11	212.5	28811.62	7	213.5	2329.15	4-6	4-10
	11	213.5	28812.11	7	214.5	2329.64	-	4-8
	12	139.5	28265.57	8	138.5	1783.10	-	5-10
	12	140.5	28265.89	8	139.5	1783.42	6-8	5-10
	16	90.5	28554.82	12	89.5	2072.35	8	8-14
	16	91.5	28555.02	12	90.5	2072.55	8-9	8-14

lines have different intensities and features depending on the e/f type of the excited level in the $D^2\Sigma^+$ state. When the transition came from an e-type level of the $D^2\Sigma^+$ state, a doublet R–Q, with the R line stronger than the Q line, was observed, and when the transition came from an f-type level, a doublet Q–P, with the P line stronger than the Q line, was observed.

It was verified that the laser pumping, generated by the frequency-doubled Ti:sapphire laser, of most of the ground state energy levels produced the excitation of a pair of $D^2\Sigma^+$ state energy levels with J'_f, $J'_e + 1$ and the same v quantum numbers. This kind of pumping behavior, which is a consequence of the similarity of the spin–rotation constant of both the $D^2\Sigma^+$ and $X^2\Sigma^+$ states, can be observed in Figs. 2, 3, and 4. The same pumping behavior was earlier observed in the laser excitation of the $E^2\Sigma^+$ state of the BaCl molecule (*27*).

Several uorescence progressions have been observed. Table 2 lists the quantum numbers J', v' and the term energy values E' of the involved $D^2\Sigma^+$ levels together with the quantum numbers

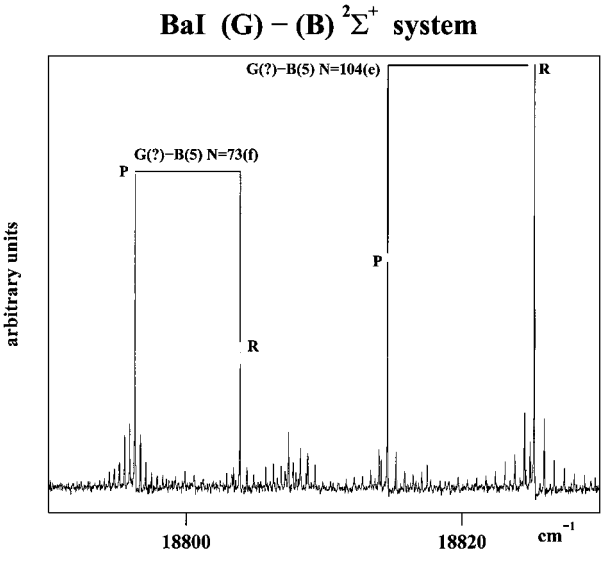

FIG. 5. Part of the G–B LIF spectrum induced by the 29 621.47 cm^{-1} Kr$^+$ laser line.

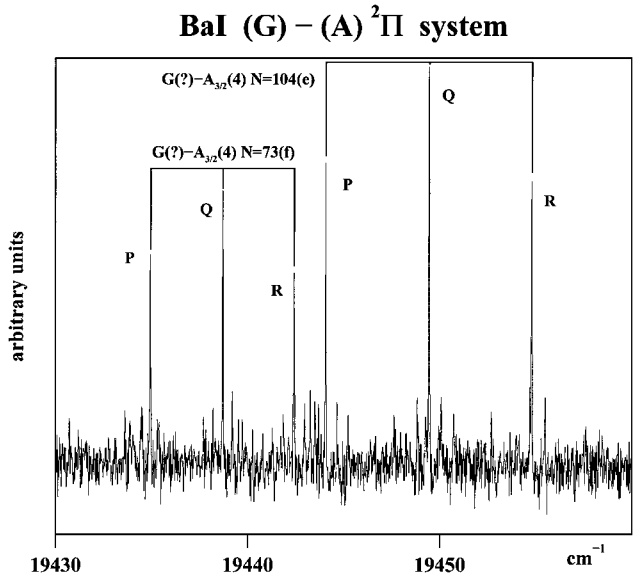

FIG. 6. Part of the G–A LIF spectrum induced by the 29 621.47 cm^{-1} Kr$^+$ laser line.

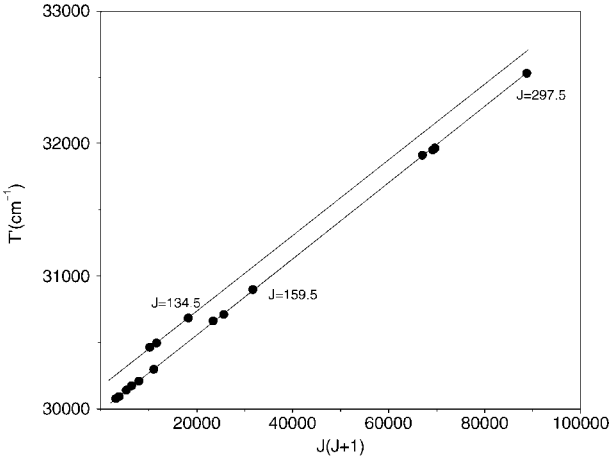

FIG. 7. Calculated term values of the G state *vs* $J(J+1)$.

J'', v'' and the term energy values E'' of the lower levels in the ground $X^2\Sigma^+$ state. The difference $v' - v''$, between the laser excited levels of the $D^2\Sigma^+$ state and the origin levels of the ground state, was always equal to 4. Table 2 shows also the range of observed vibrational levels in the $B^2\Sigma^+$ and the $A^2\Pi$ states. All the line wavenumbers were assigned to transitions involving vibrational levels up to $v' = 16$ in the $D^2\Sigma^+$ state, up to $v'' = 14$ in the $B^2\Sigma^+$ state and up to $v'' = 12$ in the $A^2\Pi$ state.

TABLE 3
Hamiltonian Energy Matrix for the $A^2\Pi$ and $C^2\Pi$ Electronic States

	$^2\Pi_{3/2}$	$^2\Pi_{1/2}$
$^2\Pi_{3/2}$	$T + A/2 + (B + A_J)(X - 1)$ $- D[(X-1)^2 + X]$ $+ H[(X-1)^3 + X(3X-1)]$ $+ (A_{JJ}/2)[3(X-1)^2 + X] + (q/2)X$	$- BX^{1/2} + 2DX^{3/2}$ $- HX^{1/2}(3X^2 + X + 1) + A_{JJ}X^{1/2}$ $+ (q/2)[X^{1/2}[-1 \pm (X+1)^{1/2}]]$ $- (p/4)X^{1/2}$
$^2\Pi_{1/2}$	sym.	$T - A/2 + (B + A_J)(X - 1)$ $- D[(X+1)^2 + X]$ $+ H[(X+1)^3 + X(3X+1)]$ $- (A_{JJ}/2)[3(X+1)^2 + X]$ $+ (q/2)[X + 2 \mp 2(X+1)^{1/2}]]$ $+ (p/2)[1 \mp (X+1)^{1/2}]$

Note. $X = (J + 1/2)^2 - 1$. Matrix elements are calculated using an e/f parity basis and are written e over f.

B. The $G^2\Sigma^+$–$A^2\Pi$ and $G^2\Sigma^+$–$B^2\Sigma^+$ Band Systems

Sixteen term levels of a $^2\Sigma^+$ state were excited using the UV laser lines of the Ar$^+$ and Kr$^+$ lasers. The usual pattern P–R of a $^2\Sigma^+$–$^2\Sigma^+$ band system can be seen in Fig. 5. From theoretical results (*7*), in which the value of the energy origin of the $G^2\Sigma^+$ state is calculated as being 30 223 cm^{-1}, it is suggested that the excited term levels concern the $G^2\Sigma^+$ electronic state. It is interesting to note that the intensity pattern of the doublets of the $G^2\Sigma^+$–$B^2\Sigma^+$ band system is the reverse of that of the $D^2\Sigma^+$–$B^2\Sigma^+$ band system. The relative intensity of the R lines was stronger than the relative intensity of the P lines when the transition came from an e-type level, and the relative intensity of the P lines was stronger than the relative intensity of the R lines when the transition came from an f-type level.

Figure 6 shows a part of the recorded spectra in which the triplet structure of the $G^2\Sigma^+$–$A^2\Pi_{3/2}$ band system can be seen. In an analogous way to the $D^2\Sigma^+$–$A^2\Pi_{3/2}$ band system, the Q lines present a relative intensity stronger than the relative intensity of the P and R lines, and the rotational relaxation lines were observed with a regular decrease in intensity. No special laser pumping behavior (like that of the $D^2\Sigma^+$ state) was observed.

IV. ANALYSIS

The obtained spectroscopic data of the $D^2\Sigma^+$–$B^2\Sigma^+$ and $G^2\Sigma^+$–$B^2\Sigma^+$ band systems, as well as that of the $D^2\Sigma^+$–$A^2\Pi$ and $G^2\Sigma^+$–$A^2\Pi$ band systems, were added to previous results (*18, 20–22*) concerning the spectroscopic data of the $A^2\Pi$–$X^2\Sigma^+$, $B^2\Sigma^+$–$X^2\Sigma^+$, $C^2\Pi$–$A^2\Pi$, $C^2\Pi$–$B^2\Sigma^+$, $C^2\Pi$–$X^2\Sigma^+$, and $C^2\Pi$–$A'^2\Delta$ band systems, and reduced by using a nonlinear least-squares method.

TABLE 4

Ar^+ and Kr^+ Multimode Ion Laser Vacuum Wavenumbers σ, Excited Term Energy Values E' of the $G^2\Sigma^+$ State Derived in the Calculations with the Respective Quantum Numbers J' (Numbers in Parentheses Represent Two Standard Deviations in Units of the Last Figure Quoted), and Quantum Numbers v'', J'' and Energy E'' of the Lower Levels in the Ground $X^2\Sigma^+$ State (Range of Observed v Values in the $A^2\Pi$ and $B^2\Sigma^+$ States)

$\sigma(cm^{-1})$	J'	$E'(cm^{-1})$	v''	$\Delta J''$	$E''(cm^{-1})$	Δv^a	Δv^b
29621.47	72.5	30140.0705(29)	2	71.5	518.56	0-8	1-10
	263.5	31966.368(18)	3	262.5	2344.84	1-8	1-8
	104.5	30296.4918(48)	2	105.5	530.00	0-7	0-10
29966.26	297.5	32530.631(21)	1	296.5	2564.77	1-7	1-7
	100.5	30462.6544(47)	1	99.5	496.92	0-10	0-10
	159.5	30712.5098(94)	0	158.5	746.73	1-6	1-6
	152.5	30662.5956(89)	0	151.5	696.68	1-6	1-6
	177.5	30900.629(11)	0	178.5	934.99	1-4	1-6
	134.5	30682.8610(73)	1	134.5	716.70	0-9	0-10
29889.31	258.5	31913.254(18)	1	259.5	2024.26	1-7	1-9
	107.5	30495.9672(52)	1	106.5	530.26	0-10	0-10
29766.76	88.5	30207.9170(39)	1	88.5	441.24	1-6	1-8
	55.5	30076.2607(24)	1	54.5	309.80	1-7	1-7
	79.5	30171.1718(34)	1	80.5	404.78	1-6	1-8
	61.5	30091.7418(26)	1	60.5	325.42	1-6	1-7
	159.5	30662.5956(89)	1	158.5	896.68	1-6	1-6
	262.5	31951.439(17)	2	158.5	2185.15	2-7	2-7

[a] $A^2\Pi$ state.
[b] $B^2\Sigma^+$ state.

The term values of the $X^2\Sigma^+$, $B^2\Sigma^+$, and $D^2\Sigma^+$ electronic states were described by standard Hund's case (b) $^2\Sigma^+$ formulae,

$$
\begin{aligned}
T &= T_v + B_v N(N+1) - D_v[N(N+1)]^2 + H_v[N(N+1)]^3 \\
&\quad + \cdots + \frac{1}{2}\gamma\ N \text{ for } e\text{-labeled levels, and} \\
&\quad - \frac{1}{2}\gamma(N+1) \text{ for } f\text{-labeled levels, with} \\
T_v &= T_e + \omega_e(v+1/2) - \omega_e x_e(v+1/2)^2 \\
&\quad + \omega_e y_e(v+1/2)^3 + \cdots \\
B_v &= B_e - \alpha_B(v+1/2) + \beta_B(v+1/2)^2 + \cdots \\
D_v &= D_e + \alpha_D(v+1/2) + \cdots \\
\gamma &= \gamma_e + \gamma_v(v+1/2) + \gamma_D N(N+1) + \cdots .
\end{aligned}
\qquad [1]
$$

The Hamiltonian matrix elements used for the isolated $C^2\Pi$ and $A^2\Pi$ electronic states are shown in Table 3. The vibrational dependence of the parameters was taken into account by a "Dunham type" variation. For example,

$$
\begin{aligned}
T_v &= T_e + \omega_e(v+1/2) - \omega_e x_e(v+1/2)^2 \\
&\quad + \omega_e y_e(v+1/2)^3 + \cdots \\
A &= A_e + A_v(v+1/2) + A_{vv}(v+1/2)^2 + \cdots \\
B_v &= B_e - \alpha_B(v+1/2) + \beta_B(v+1/2)^2 + \cdots \\
D_v &= D_e + \alpha_D(v+1/2) + \cdots \\
p &= p_e + p_v(v+1/2) + p_J J(J+1) + \cdots \\
&\quad + p_{vv}(v+1/2)^2 + \cdots .
\end{aligned}
\qquad [2]
$$

TABLE 5

Molecular Constants in cm^{-1} for the $X^2\Sigma^+$, $B^2\Sigma^+$, and $D^2\Sigma^+$ Electronic States Determined in the Analysis from a Nonlinear Least-Squares Fit of the Global Data Set (Numbers in Parentheses Represent Two Standard Deviations in Units of the Last Figure Quoted)

coeff.	$X^2\Sigma^+$	$B^2\Sigma^+$	$D^2\Sigma^+$
T_e[a]	[0]	10427.02271(58)	25775.11128(114)
$B_e \times 10^{+2}$	2.6804551(465)	2.6113433(466)	2.8088703(894)
$D_e \times 10^{+9}$	3.31357(571)	3.52044(578)	2.9373(216)
$H_e \times 10^{+16}$	-1.640(231)	-2.853(234)	-8.535(758)
$\alpha_B \times 10^{+5}$	6.635018(987)	7.24250(113)	7.2232(210)
$\beta_B \times 10^{+8}$	3.4177(663)	5.0182(563)	-67.51(182)
$\gamma_B \times 10^{+11}$	8.21(172)	12.39(258)	781.7(511)
$\alpha_D \times 10^{+12}$	1.5323(563)	2.1921(655)	82.56(400)
$\beta_D \times 10^{+12}$	-	-	-2.673(202)
ω_e	152.163175(272)	141.951547(292)	161.3901991(512)
$\omega_e x_e$	0.2726744(230)	0.2896530(276)	0.36421456(101)
$\omega_e y_e \times 10^{+4}$	2.37212(590)	3.11148(776)	-17.0374409(340)
$\gamma_e \times 10^{+3}$	2.53620(222)	-56.40752(401)	2.123762652(14)
$\gamma_J \times 10^{+10}$	-3.749(208)	116.781(581)	-0.0557462(892)
$\gamma_{JJ} \times 10^{+14}$	-	-	3.693(389)
$\gamma_v \times 10^{+5}$	-1.1230(215)	8.2267(310)	3.536(208)
$\gamma_{vv} \times 10^{+6}$	-	-	-2.231(165)

[a] Origin of the energies at the level $v = -1/2$, $N = 0$ of the ground state, same origin as in Tables 4, 6 and 7.

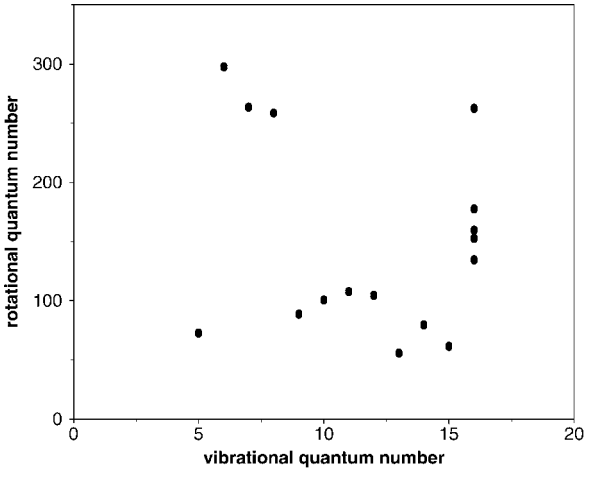

FIG. 8. Schematic representation of the *D* state data set used in the analysis of the observed wavenumbers.

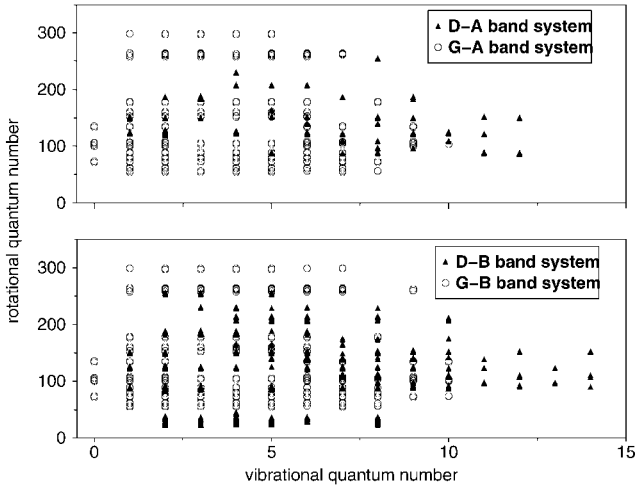

FIG. 9. Schematic representation of the data for both the *A* and *B* state sets used in the analysis of the observed wavenumbers.

TABLE 6

Molecular Constants in cm^{-1} for the $A'^2\Delta$, $A^2\Pi$, and $C^2\Pi$ Electronic States Determined in the Analysis from a Nonlinear Least-Squares Fit of the Global Data Set (Numbers in Parentheses Represent Two Standard Deviations in Units of the Last Figure Quoted)

coeff.	$A'^2\Delta_{3/2}$	$A^2\Pi$	$C^2\Pi$
T_e	8369.0381(143)	9605.423748(652)	18188.50700(43)
$B_e \times 10^{+2}$	2.623438(122)	2.59470737(109)	2.6726955(493)
$D_e \times 10^{+9}$	5.0929(311)	3.46379(588)	3.05971(594)
$H_e \times 10^{+16}$	93.84(278)	-2.454(250)	-1.425(233)
$\alpha_B \times 10^{+5}$	6.93524(231)	7.0235(355)	6.359995(986)
$\beta_B \times 10^{+8}$	4.4887(972)	3.4830(539)	2.7166(438)
$\alpha_D \times 10^{+12}$	2.579(117)	2.561(137)	1.8343(593)
$A_e \times 10^{-2}$	-	6.5665507(105)	7.56059904(667)
$A_J \times 10^{+6}$	-	-37.5060(163)	-4.0333(187)
$A_{JJ} \times 10^{+12}$	-	-7.396(757)	4.6673(610)
$A_v \times 10^{+1}$	-	-5.24796(287)	1.09706(202)
$A_{vv} \times 10^{+3}$	-	2.3199(134)	1.5993(140)
$A_{vj} \times 10^{+7}$	-	1.4055(767)	3.8049(154)
ω_e	142.285880(908)	141.747957(410)	157.795574(387)
$\omega_e x_e$	0.2741056(628)	0.2753768(455)	0.2747645(522)
$\omega_e y_e \times 10^{+4}$	2.6083(189)	2.4094(147)	2.1759(227)
$p_e \times 10^{+2}$	-	-5.61110(160)	0.703091(554)
$p_J \times 10^{+8}$	-	1.3272(481)	-0.32291(493)
$p_v \times 10^{+5}$	-	7.226(158)	-4.3510(410)
$q_e \times 10^{+5}$	-	2.587(193)	-0.2022(450)
$q_J \times 10^{+11}$	-	-	1.374(284)
$q_v \times 10^{+6}$	-	2.682(706)	-

TABLE 7

Comparison between the Theoretical Values of Transition Energies (in cm^{-1}) and Those Calculated in This Work (Numbers in Parentheses Represent Two Standard Deviations in Units of the Last Figure Quoted)

State	This work	Allouche *et al.* [5]	Törring *et al.* [1]	Raoufi *et al.* [7]
$A'^2\Delta$	8699($T_{3/2} + A_{calc.}$)	8273	8780	8297
$A^2\Pi$	9605.423748(652)	9300	9420	9575
$B^2\Sigma^+$	10427.02271(58)	10003	10160	10584
$C^2\Pi$	18188.50700(43)	21528	21220	18330
$D^2\Sigma^+$	25775.11128(114)	-	-	25291

The term values concerning the $A'^2\Delta_{3/2}$ states were described by standard Hamiltonian representations (see, for example, (*27*)). Considering that only one component of the $A'^2\Delta_{3/2}$ state was observed, the spin–orbit dependence could not be determined. Vibrational dependence of parameters was taken into account by a Dunham type variation.

The 16 term values of the $G^2\Sigma^+$ state were kept as free parameters and determined in the calculations. Figure 7 shows a schematic diagram representing the term levels of the $G^2\Sigma^+$ state vs $J(J+1)$. In Fig. 7 it can also be observed that the term levels concern 2 undetermined, and probably consecutive, vibrational levels. Table 4 lists the term energy values E' of the $G^2\Sigma^+$ state, derived from the calculations, together with the quantum numbers J'', v'' and the term energy values E'' of the lower levels in the ground state. Table 4 shows also the range of observed vibrational levels in the $B^2\Sigma^+$ and $A^2\Pi$ states. All the line wavenumbers were assigned to transitions involving, as previously mentioned, 2 undetermined vibrational levels of the $G^2\Sigma^+$ state, 11 vibrational levels (up to $v''=10$) in the $B^2\Sigma^+$ state, and 11 vibrational levels (up to $v''=10$) in the $A^2\Pi$ state.

Figure 8 shows a schematic diagram of the analyzed vibrational and rotational data field of the $D^2\Sigma^+$ state through the D–A and D–B band systems. Figure 9 shows the range of the observed v and J in the $A^2\Pi$ and $B^2\Sigma^+$ electronic states through the D–A, D–B, G–A, and G–B band systems. Several transitions involving previously unobserved vibrational levels of both the $A^2\Pi_{1/2}$ component ($v''=6$) and the $A^2\Pi_{3/2}$ component ($v''=6, 8, 11, 12$) could be assigned, complementing the previously analyzed data set (*21*).

Table 5 summarizes the final values of the recommended effective molecular constants for the ground, $B^2\Sigma^+$, and $D^2\Sigma^+$ electronic states, respectively, derived from the global analysis described above. In the same way, Table 6 summarizes the final values of the recommended effective molecular constants for the $A'^2\Delta_{3/2}$ component, $A^2\Pi$, and $C^2\Pi$ electronic states, derived from the global analysis. The standard deviation was less than 3.3×10^{-3} cm^{-1}. Very minor differences exist with our previously reported molecular parameters.

Table 7 shows the energy origins obtained in this work for the $A'^2\Delta$, $A^2\Pi$, $B^2\Sigma^+$, $C^2\Pi$, and $D^2\Sigma^+$ electronic states, as well as the theoretical values for the same constants derived from the model of the *ligand field approach* (*5*), from the model of *electrostatic polarization* (*1*), and from the *generalized quantum defect theory* (*7*). The $A'^2\Delta$ energy origin obtained in this work is in fact equal to $T-A$, where A represents the spin–orbit constant of the state. The value of this parameter was calculated (*6*) to be about 330 cm^{-1}. On the whole, the energy origin values obtained by using the quantum defect theory present a better agreement with the experimental values obtained in this work than those, obtained by using both the ligand field approach method and the electrostatic polarization method. The energy origin of the $A'^2\Delta$ state is an exception: the obtained value calculated using the ligand field approach method presents a better agreement with the experimental value obtained in this work.

V. CONCLUSION

Laser-induced fluorescence (LIF) combined with Fourier transform spectroscopy (FTS) has allowed the first spectroscopic study with rotational resolution of the $D^2\Sigma^+$ and probably the $G^2\Sigma^+$ electronic state of the BaI molecule. The data previously published in (*18, 20–22*) were added to the present work data set and a global analysis was performed. The global data set concerns seven electronic states and 10 band systems ($A^2\Pi$–$X^2\Sigma^+$, $B^2\Sigma^+$–$X^2\Sigma^+$, $C^2\Pi$–$X^2\Sigma^+$, $C^2\Pi$–$A'^2\Delta$, $C^2\Pi$–$A^2\Pi$, $C^2\Pi$–$B^2\Sigma^+$, $D^2\Sigma^+$–$A^2\Pi$, $D^2\Sigma^+$–$B^2\Sigma^+$, $G^2\Sigma^+$–$A^2\Pi$, and $G^2\Sigma^+$–$B^2\Sigma^+$) including 116 vibrational levels of all the seven involved electronic states. The analyzed transitions hold a rotational range between $J=4.5$ and $J=531.5$. An improved set of 152 molecular constants and also 16 term values (of the G state) were calculated, which reproduced all the 12 684 analyzed transitions with a standard deviation of 3.26×10^{-3} cm^{-1}.

ACKNOWLEDGMENTS

This work is partially supported by CAPES/COFECUB (Brazil/France cooperation) 182/96. The authors are grateful to Mrs. J. Chevillard for her skillful help during the recording of the spectra.

REFERENCES

1. T. Törring, W. E. Ernst, and S. Kindt, *J. Chem. Phys*. **90,** 4927–4932 (1989).
2. T. Törring, W. E. Ernst, and J. Kändler, *J. Chem. Phys*. **81,** 4614–4619 (1984).
3. S. F. Rice, H. Martin, and R. W. Field, *J. Chem. Phys*. **82,** 5023–5034 (1985).
4. M. Arif, Ch. Jungen, and A. L. Roche, *J. Chem. Phys*. **106,** 4102–4118 (1997).
5. A. R. Allouche, G. Wannous, and M. Aubert-Fréecon, *Chem. Phys*. **170,** 11–22 (1993).
6. A. R. Allouche, Thèse de Doctorat, Université Claude-Bernard Lyon I, 1993.
7. S. Raoufi and C. Jungen, to be published (2000).
8. O. H. Walters and S. Barratt, *Proc. R. Soc. London Ser. A* **118,** 120–137 (1928).
9. P. Mesnage, *Ann. Phys*. **12,** 5–9 (1939)
10. M. M. Patel and N. R. Shah, *Ind. Appl. Phys*. **8,** 681–682 (1970).
11. M. L. P. Rao, D. V. K. Rao, P. T. Rao, and P. S. Murty, *Fizika* **9,** 25–29 (1977).
12. R. S. Bradford, Jr., C. R. Jones, L. A. Southall, and H. P. Broida, *J. Chem. Phys*. **62,** 2060–2064 (1975).
13. M. A. Johnson, C. R. Webster, and R. N. Zare, *J. Chem. Phys*. **75,** 5575–5577 (1981).
14. M. A. Johnson and R. N. Zare, *J. Chem. Phys*. **82,** 4449–4459 (1985).
15. M. A. Johnson, C. Noda, J. S. McKillop, and R. N. Zare, *Can. J. Phys*. **62,** 1467–1477 (1984).
16. D. Zhao, P. H. Vaccaro, A. A. Tsekouras, C. A Leach, and R. N. Zare, *J. Mol. Spectrosc*. **148,** 226–242 (1991).
17. C. A Leach, J. R. Waldeck, C. Noda, J. S. McKillop, and R. N. Zare, *J. Mol. Spectrosc*. **146,** 465–492 (1991).
18. C. A. Leach, A. A. Tsekouras, and R. N. Zare, *J. Mol. Spectrosc*. **153,** 59–72 (1992).

19. T. Töring and K. Döbl, *Chem. Phys. Lett*. **115,** 328–332 (1985).
20. R. F. Gutterres, J. Vergès, and C. Amiot, *J. Mol. Spectrosc*. **196,** 29–44 (1999).
21. R. F. Gutterres, J. Vergès, and C. Amiot, *J. Mol. Spectrosc*. **200,** 253–260 (2000).
22. R. F. Gutterres, J. Vergès, and C. Amiot, *J. Mol. Spectrosc*. **201,** 326–327 (1999).
23. C. R. Vidal and J. Cooper, *J. Appl. Phys*. **40,** 3370–3374 (1969).
24. C. Amiot and J. Vergès, *Chem. Phys. Lett*. **185,** 310–312 (1991).
25. C. Amiot, M. Hafid, and J. Vergès, *J. Phys. B* **26,** L407–L412 (1993).
26. M. Hafid, C. Amiot, and J. Vergès, *Chem. Phys. Lett*. **210,** 45–49 (1993).
27. C. Amiot, M. Hafid, and J. Vergès, *J. Mol. Spectrosc*. **180,** 121–138 (1996).
28. O. Launila and P. Royen, *Mol. Phys*. **82,** 815–823 (1994).
29. A. Bernard, C. Effantin, E. Andrianavalona, J. Vergès, and R. F. Barrow, *J. Mol. Spectrosc*. **152,** 174–178 (1992).
30. Z. J. Jakubek and R. W. Field, *Phys. Chem. Lett*. **72,** 2167–2170 (1994).
31. C. M. Gittins, N. A. Harris, R. W. Field, J. Vergès, C. Effantin, A. Bernard, J. d'Incan, W. E. Ernst, P. Bündgen, and B. Engels, *J. Mol. Spectrosc*. **161,** 303–311 (1993).